ACS OMEGA

http://pubs.acs.org/journal/acsodf

Article

Functional Pyromellitic Diimide as a Corrosion Inhibitor for Galvanized Steel: An Atomic-Scale Engineering

Anoop Kumar Kushwaha,[‖] Mihir Ranjan Sahoo,[‖] Mausumi Ray,[‖] Debashish Das, Suryakanta Nayak, Apurba Maity, Kuntal Sarkar, Amar Nath Bhagat, Atanu Ranjan Pal, Tapan Kumar Rout, and Saroj Kumar Nayak*

Cite This: https://doi.org/10.1021/acsomega.2c01299

Read Online

ACCESS | Metrics & More | Article Recommendations

ABSTRACT: Corrosion of metal/steel is a major concern in terms of safety, durability, cost, and environment. We have studied a cost-effective, nontoxic, and environmentally friendly pyromellitic diimide (PMDI) compound as a corrosion inhibitor for galvanized steel through density functional theory. An atomic-scale engineering through the functionalization of PMDI is performed to showcase the enhancement in corrosion inhibition and strengthen the interaction between functionalized PMDI (F-PMDI) and zinc oxide (naturally existing on galvanized steel). PMDI is functionalized with methyl/diamine groups (inh1 (R = $-CH_3$, R′ = $-CH_3$), inh2 (R = $-CH_3$, R′ = $-CH_2CH_2NH_2$), and inh3 (R = $-C_6H_3(NH_2)_2$, R′ = $-CH_2CH_2NH_2$). The corrosion inhibition parameters (e.g., orbital energies, electronegativity, dipole moment, global hardness, and electron transfer) indicate the superior corrosion inhibition performance of inh3 (inh3 > inh2 > inh1). Inh3 (~182.38 kJ/mol) strongly interacts with ZnO($10\bar{1}0$) compared to inh2 (~122.56 kJ/mol) and inh1 (~119.66 kJ/mol). The superior performance of inh3 has been probed through charge density and density of states. Larger available states of N and H (of inh3) interact strongly with Zn and O_{surf} (of the surface), respectively, creating N−Zn and H−O_{surf} bonds. Interestingly, these bonds only appear in inh3. The charge accumulation on O_{surf}, and depletion on H(s), further strengthens the bonding between inh3 and ZnO(1010). The microscopic understanding obtained in this study will be useful to develop low-cost and efficient corrosion inhibitors for galvanized steel.

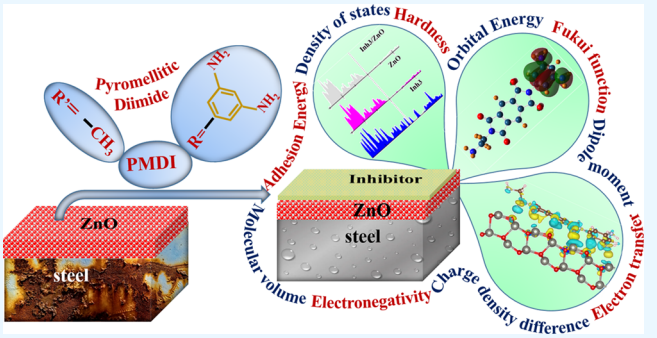

1. INTRODUCTION

Galvanized steel (zinc-coated steel) is widely used in several industries due to its durability, sustainability, cost-effectiveness, high mechanical strength, rust resistance, sacrificial anodes (initially coated zinc will corrode on exposure to the environment), and so forth.[1] During manufacturing, a continuous hot-dip galvanizing process provides a tight bonding between the coated zinc and steel. Almost entire zinc (>99%) is present in the coating composition. A thin layer of zinc oxide (ZnO) formed on the coated zinc surface on exposure to the atmosphere. Also, atomic layer deposition of the ZnO thin film on the steel surface provides good structural and thermal stability.[2,3] The ZnO film forms zinc hydroxide on contact with water/humidity and finally forms zinc carbonate on exposure to atmospheric carbon dioxide. Zinc carbonate is highly insoluble in water and forms a gray film on the surface. This gray film impedes further chemical changes and prevents oxygen and moisture from reaching the steel beneath. Thus, coating on the steel inhibits the rusting of galvanized steel. However, in extreme conditions, for example, high humidity, sodium chloride (salted water), sulfur dioxide pollution, strong alkalis, acid rainwater, and so forth, zinc carbonate breaks, resulting in heavy corrosion.[1,4,5] Corrosion of metal/steel is a major concern in terms of safety, durability, cost, and environment.[6−8] Generally, the corrosion resistance performance of galvanized steel enhances with the increasing coating layer/thickness. However, the fracture properties are developed after a certain layer/thickness, which destabilize the coating.[9] Therefore, an alternative method is highly required to protect the galvanized steel from corrosion.

Numerous inhibitors have been developed to protect the mild/galvanized steel through controlling the corrosion reaction either by physically blocking the surface or by altering the energy barrier.[10−13] These inhibitors bind/adhere on the metallic surface and form a protective film. This thin film prevents the interaction between corrosive agents and the metallic surface. The inhibitor's effectiveness and efficiency against corrosion are directly associated with its electronic

Received: March 4, 2022
Accepted: July 8, 2022

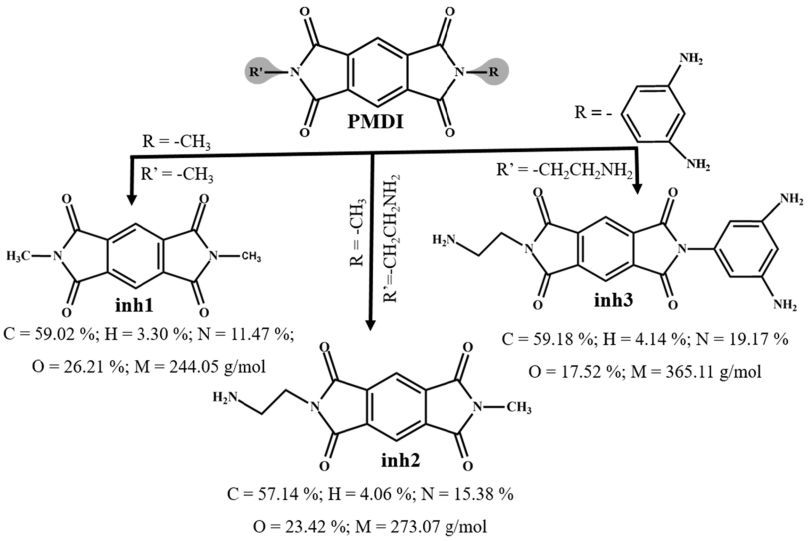

Figure 1. Schematic structure of PMDI and its respective functional inhibitors. The elemental composition and molar mass (M) of functional PMDI (F-PMDI) inhibitors are given at the bottom of the structures.

properties as well as binding with a metallic surface. The interaction occurs through either donation of electrons from the inhibitor to unoccupied d-orbitals (of the metallic surface) or acceptance of free electrons (of the metallic surface) by the inhibitor with antibonding orbitals.[14] The electrostatic interaction represents physical adsorption, while charge sharing/transfer shows the chemical adsorption between the inhibitor and the metallic surface. Previous studies found that organic inhibitors containing N, O, and S show better inhibition efficiency.[15,16] These heteroatoms have a donor site that forms an unsaturated bond with the planar conjugated aromatic inhibitor molecules. Further, heteroatoms have an excellent capability to donate the available lone-pair electrons and form multiple bonds by adsorption on the metal surface. Thus, the inhibitor molecule containing heteroatoms works as a superior potential barrier and effectively prevents the metal's surface from corrosion. The organic molecule derived from piperidine, quinolone, triazoles, quinazolinone, pyrimidinone, and so forth is an efficient corrosion inhibitor for mild steel.[17−22] Inhibitors based on phosphate-/calcium-ion inhibitor mixture, sol−gel coating materials, decanoic acid, organosilane, benzotriazole, and so forth have been developed for galvanized steel.[23−27] However, developing a cost-effective, high corrosion-resistant, nontoxic, and environmentally friendly corrosion inhibitor for galvanized steel is still a highly challenging topic for researchers.

Low cost, greater electron donation/acceptance capability, and excellent ability to form polyimide polymers suggest that pyromellitic diimide (PMDI) can be used as a corrosion inhibitor.[28,29] However, the weak interaction of PMDI with metallic surfaces is of primary concern. The molecule adsorption on mild steel (iron surface) is generally greater than that on galvanized steel (ZnO surface). The Fe atom has incomplete sublevels in mild steel, while the surface Zn atom has complete sublevels in galvanized steel. Therefore, adsorption occurs only due to electron exchange, leading to weak interaction on the ZnO surface. However, interaction/binding could be enhanced by either selecting suitable inhibitors or modifying/engineering inhibitor molecules at the atomic level. Ebenso et al. have found superior corrosion inhibition performance for functionalized tetrahydropyridines compared to the pristine part with both theoretical and experimental methods.[30] Galai et al. have studied functionalized hydroxyquinoline derivatives as corrosion inhibitors for mild steel.[31] Earlier, inhibitors based on amino- and carboxylic acid groups have been studied on the ZnO surface.[32,33] The presence of O, S, N, and pi bonds and high electron density provides an initial guess for selecting inhibitors, although the exact atomic-level understanding is still lacking.

In the present work, we have functionalized PMDI to be used as a corrosion inhibitor for galvanized steel. As shown in Figure 1, the functionalized PMDI (F-PMDI) is defined with inh1 (R = $-CH_3$, R′ = $-CH_3$), inh2 (R = $-CH_3$, R′ = $-CH_2CH_2NH_2$), and inh3 (R = $-C_6H_3(NH_2)_2$, R′ = $-CH_2CH_2NH_2$). Through molecular orbital formalism-based density functional theory (DFT) and polarizable continuum model (PCM), we have investigated corrosion resistance parameters such as orbital energies, global hardness, and the fraction of electron transferred of F-PMDI inhibitors in gaseous as well as aqueous phase. The obtained results show a superior corrosion inhibition performance for inh3, followed by inh2 and inh1 (i.e., in the order of inh3 > inh2 > inh1). Further, we have studied the adsorption of F-PMDI on the ZnO$(10\bar{1}0)$ surface with first-principles density functional theory. Inh3 strongly adsorbed on the ZnO$(10\bar{1}0)$ surface, found as an efficient candidate for corrosion inhibition. The origin of the superior performance of inh3 has been probed through density of states and charge density difference, thereby providing an atomic-level understanding of the interaction of the corrosion inhibitor with surfaces. We provide the theoretical and computational details in the next section.

2. THEORETICAL AND COMPUTATIONAL DETAILS

The ionization potential ($I = -E_{HOMO}$) and electron affinity ($A = -E_{LUMO}$) are directly related to the highest occupied molecular orbital (HOMO) and lowest unoccupied molecular orbital (LUMO), respectively, as per Koopman's theorem. The electronegativity (χ), global hardness (η), and softness ($\sigma = (1/\eta)$) are computed with the following equations;

$$\chi = \frac{I + A}{2}; \eta = \frac{I - A}{2}$$

https://doi.org/10.1021/acsomega.2c01299
ACS Omega XXXX, XXX, XXX−XXX

The global electrophilicity index, ($\omega = (\chi^2)/2\eta$), and nucleophilicity, ($\varepsilon = 1/\omega$), also provide vital information about the inhibitor efficiency. The fraction of electrons transferred (ΔN) from the inhibitors to the surface and vice versa could be calculated with the following expression

$$\Delta N = \frac{\Phi - \chi_{inh}}{2(\eta_{ZnO} + \eta_{inh})}$$

where Φ and η_{ZnO} are the work function and global hardness of the ZnO($10\bar{1}0$) surface, while χ_{inh} and η_{inh} are the electronegativity and global hardness of the inhibitors, respectively. The work function of the ZnO($10\bar{1}0$) surface is selected as 4.71 eV based on an earlier report.[34]

The local reactivity has been investigated with the Fukui function, representing the inhibitor molecule's reactive centers. Concerning the finite difference approximation, the Fukui functions of k'th atom having "n" electrons are obtained with the following relations;

$$f^+ = q_k(n) - q_k(n+1) \text{ for nucleophilic attack}$$

$$f^- = q_k(n-1) - q_k(n) \text{ for electrophilic attack}$$

where $q_k(n)$, $q_k(n+1)$, and $q_k(n-1)$ are the charges of the k'th atom for n, $n+1$, and n-1 electron systems, respectively.

The adsorption energy (E_{ads}) has been calculated with the following equation

$$E_{ads} = E_{total} - (E_{slab} + E_{inhibitor})$$

where E_{total}, E_{slab}, and $E_{inhibitor}$ represent the energy of the combined inhibitor/ZnO($10\bar{1}0$) system, ZnO($10\bar{1}0$) slab, and F-PMDI inhibitors.

The electronic, molecular, and chemical properties of F-PMDI have been explored with the molecular orbital formalism-based density functional theory (DFT). The high accuracy of the computed parameters and short time lead to the proficient technique for theoretical investigations. The geometrical optimization (in both gaseous and aqueous phases) has been carried out with a hybrid B3LYP functional set and a diffused and polarized 6-311+G(d,p) basis set.[35,36] With nonpolarized spin and convergence parameters (average distance, 1.2×10^{-3} Bohr, and average force, 3×10^{-4} Hartree/Bohr over all atoms), the structures are fully optimized with the Gaussian 09 code.[37] The conductor-like polarizable continuum model (CPCM) is used to analyze the effect of water on the electronic properties as well as the corrosion resistance parameters of inhibitors. In this model, the aqueous medium is defined with the dielectric constant (ε = 78.35 for water). The absence of the imaginary mode in the vibrational spectra confirms the local minimum energy on the potential energy surface. The molecular orbitals' energy distribution and electrostatic potential surface have been mapped with GaussView.

The DFT-based Vienna ab initio simulation package (VASP) code is used to perform geometrical relaxation and electronic structure calculations of F-PMDI on the ZnO($10\bar{1}0$) surface.[38,39] In the present work, the Perdew–Burke–Ernzerhof (PBE) version of generalized gradient approximation (GGA) is considered as the exchange–correlation functional.[40−42] The projector augmented-wave (PAW) method is employed with a kinetic energy cutoff of 500 eV to describe the plane-wave basis set. The F-PMDI inhibitors are adsorbed on a two-layered ZnO($10\bar{1}0$) slab having 48 atoms (24 Zn and 24 O atoms) per layer. The size of the supercell of ZnO($10\bar{1}0$) is considered as 9.86Å × 21.20Å × 25.7 Å in a sufficient vacuum for F-PMDI. For the ZnO($10\bar{1}0$) surface and the ZnO/inhibitor systems, a vacuum of 20 Å is introduced along the z-direction to curtail the interactions between images created due to periodicity. A 4 × 2 × 1 grid within the Monkhorst–Pack scheme is chosen to sample the Brillouin zone for non-spin-polarized self-consistent calculations.[43] The free F-PMDI inhibitors are modeled in a large vacuum box which provides sufficient vacuum in all directions to avoid the image interactions. Only one gamma point is used to perform the k-point integration for the nonperiodic inhibitors. Further, convergence parameters, namely, self-consistent field (SCF) energy and Hellmann–Feynman force, are fixed at 10^{-4} eV and 10^{-3} eV/Å, respectively, over each atom. The van der Waals correction is included by using Grimme's DFT-D2 method. This is a reasonable choice for maintaining a balance between the computational cost and correction of the adsorption energies of the inhibitors interacting with the ZnO($10\bar{1}0$) surface.

3. RESULTS AND DISCUSSION

3.1. F-PMDI Inhibitors. The schematic picture, element percentage ratio, and molar mass of F-PMDI inhibitors, for example, inh1 (R = $-CH_3$, R′ = $-CH_3$), inh2 (R = $-CH_3$, R′ = $-CH_2CH_2NH_2$), and inh3 (R = $-C_6H_3(NH_2)_2$, R′ = $-CH_2CH_2NH_2$) are shown in Figure 1. The element percentage ratio of carbon (57.14–59.18%) and hydrogen (3.30–4.14%) in the inhibitors does not show significant variation. The element ratio of nitrogen enhances from inh1 (11.47%) to inh2 (15.38%) to inh3 (19.17%), while that of oxygen reduces from inh1 (26.21%) to inh2 (23.42%) to inh3 (17.52%). The excess oxygen of the inhibitor may be repulsive with the surface oxygen, resulting in weak adsorption. At the same time, excess nitrogen in the inhibitor donates more σ-electrons to the surface and forms a donor–acceptor complex, resulting in strong adsorption. The molar mass of inh1, inh2, and inh3 is 244.05, 273.07, and 365.11 g/mol, respectively, and increases from inh1 to inh3.

To determine the electronic properties (i.e., ionization potential, electron affinity, chemical reactivity, etc.) of F-PMDI inhibitors, we have optimized the structures (shown in Figure 2) at the B3LYP/6-311+G(d,p) level. inh1 is planar, while the chain R = $-CH_2CH_2NH_2$ in inh2 has an angle of 112.54° (∠NCC) with the aromatic planar structure. In inh3, the aromatic diamine group is tilted (42.41°) compared to the planar PMDI. The orbital density distribution (shown in Figure 2) shows that LUMO is distributed over the PMDI structure while HOMO is spread over the whole structure (in inh1), localized on the aliphatic amine (R = $-CH_2CH_2NH_2$) group (in inh2) and on the aromatic diamine group (in inh3). Thus, the HOMO distribution localized on the functional group (in inh2 and inh3) controls the electronic properties of F-PMDI. The electrostatic potential (ESP) mapped on the electron density surfaces (Figure 2) is represented by the blue and red regions for electron-deficient and excess electron areas, respectively. During the adhesion of inhibitors on the ZnO($10\bar{1}0$) surface, the bonds are formed either in the electron-deficient (blue) region (through accepting electrons) or in the electron excess (red) region (through donating electrons). The electron excess/deficient regions are formed near nitrogen and oxygen atoms in the F-PMDI inhibitors.

https://doi.org/10.1021/acsomega.2c01299
ACS Omega XXXX, XXX, XXX−XXX

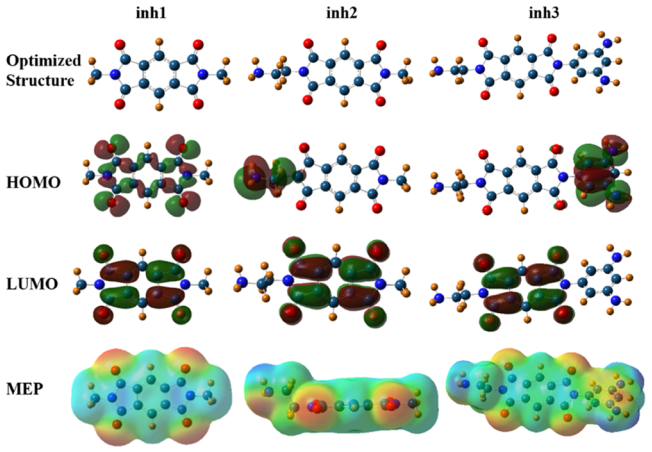

Figure 2. Optimized geometrical structures, isodensity surface plot of HOMO and LUMO (isosurface value, 0.02), and molecular electrostatic potential (MEP) of inh1 (left panel), inh2 (middle panel), and inh3 (right panel). For MEP, the limiting values of blue and red regions are +0.049 and −0.049, respectively. Red, brown, light blue, and dark blue sphere represent oxygen, hydrogen, nitrogen, and carbon atoms, respectively.

Therefore, their elemental composition highly impacts the inhibitor adsorption on the ZnO$(10\bar{1}0)$ surface.

The ionization potential ($I = -E_{HOMO}$), electron affinity ($A = -E_{LUMO}$), and HOMO−LUMO energy gap (ΔE_{gap}) provide the vital information about reactivity, as listed in Table 1. I, A, and ΔE_{gap} show decrement from inh1 to inh3, with the lowest value for inh3. The lowest ΔE_{gap} shows the highest reactivity; therefore, inh3 (ΔE_{gap} = 2.28 eV) is found as a superior inhibitor. The electron-donating ability of the inhibitor is measured by electronegativity (χ). The inhibitor with lower χ (higher electron-donating propensity) provides an efficient restraining proficiency. χ is more inadequate for inh3 (χ = 4.19 eV) and shows greater restraining ability, making it suitable for corrosion inhibition. The inhibitor stability and reactivity have been further probed through absolute hardness (η), which implies the resistance toward polarization/deformation of electron cloud with minor changes in the reaction. For an efficient inhibitor, η must be small (i.e., large softness (σ) value). The η (σ) value (listed in Table 1) decreases (increases) in the order inh1 > inh2 > inh3. The least η (1.14 eV) and greatest σ (0.88 eV^{-1}) make inh3 an efficient inhibitor. The η value of inh3 is consistent with ΔE_{gap} as hard molecules have a large band gap. An inhibitor with large σ implies an easy electron transfer to/from the surface. The electrons are transferred easily to/from inh3 due to the high σ (0.88 eV^{-1}) value. The nonuniform distribution of charges on inhibitors is estimated by the dipole moment (μ). Large μ indicates high deformation energy and hence greater adsorption efficiency. Inh3 has a comparatively larger μ (2.26 D; Table 1), providing greater adsorption efficiency.

The inhibitors with large surface/volume (estimated with the van der Waals (vdW) volume) have more contact regions for interaction with the surface. The large contact regions of inhibitors cover a greater area of the ZnO$(10\bar{1}0)$ surface, protecting the maximum surface from corrosion. The vdW volume, calculated with the Monte−Carlo method, based on multiwfn code[44] and listed in Table 1, showed that inh3 (400.36 $Å^3$) has comparatively greater volume then inh1 (250.98 $Å^3$) and inh2 (296.35 $Å^3$). Thus, inh3 provides a large contact area for adsorption, leading to a superior inhibitor performance. The electron acceptance/donation ability of an inhibitor is estimated with electrophilicity index (ω) and nucleophilicity index (ε). The larger ω and ε values imply a greater ability to accept/donate electrons; hence, inh3 (ω = 7.70 eV; Table 1) was found to be a superior electrophilic inhibitor. The inhibitor reactivity and active centers are further studied through back-donation ($\Delta E_{back\text{-}donation}$). If $\eta > 0$ and $\Delta E_{back\text{-}donation} < 0$, $\Delta E_{back\text{-}donation}$ implies charge transfer to the inhibitor, followed by the back-donation from the inhibitor. $\Delta E_{back\text{-}donation}$ is energetically favored for inh3 (−0.29 eV; Table 1) compared to inh1 (−0.56 eV) and inh2 (−0.45 eV). The fraction of electron transfer (ΔN) represents inhibition efficiency in terms of electron donation capability. The electron-donating ability enhances with an increment in ΔN (up to 3.6). A negative (positive) sign implies that a fraction of electron transfer occurs from the surface to the inhibitor (inhibitor to the surface). The negative ΔN values (listed in Table 1) for inh1 (−0.120) and inh2 (−0.025) represent that the fraction of electron is transferred to the surface. A positive

Table 1. Computed Numerical Values of Quantum Chemical Parameters of Functional PMDA Corrosion Inhibitors in Gaseous as well as Aqueous Media

quantum chemical parameters	inh1		inh2		inh3	
	gas	water	gas	water	gas	water
E_{HOMO} (eV)	−7.61	−7.45	−6.69	−6.63	−5.34	−5.26
E_{LUMO} (eV)	−3.16	−3.06	−3.14	−3.09	−3.05	−3.01
energy band gap (ΔE_{gap}; eV)	4.45	4.39	3.56	3.54	2.28	2.25
ionization potential (I; eV)	7.61	7.45	6.69	6.67	5.34	5.26
electron affinity (A; eV)	3.16	3.06	3.14	3.07	3.05	3.01
absolute electronegativity (χ; eV)	5.38	5.26	4.92	4.87	4.19	4.13
hardness (η; eV)	2.23	2.19	1.78	1.80	1.15	1.13
softness (σ; eV^{-1})	0.45	0.46	0.56	0.55	0.87	0.88
dipole moment (μ; Debye)	0.63	0.07	1.49	1.87	2.26	2.97
electrophilicity ω (eV)	6.98	6.29	6.79	6.58	7.70	7.55
nucleophilicity ε $(eV)^{-1}$	0.14	0.16	0.15	0.15	0.13	0.13
fraction of electron transferred, ΔN	−0.120	−0.094	−0.025	−0.013	0.246	0.261
$\Delta E_{back\text{-}donation}$ (eV)	−0.56	−0.55	−0.45	−0.44	−0.29	−0.28
molecular volume (vdW; $Å^3$)	250.98		296.35		400.36	
E_{ads} (kJ/mol)	−119.66		−122.56		−182.38	

https://doi.org/10.1021/acsomega.2c01299
ACS Omega XXXX, XXX, XXX−XXX

Table 2. Computed Numerical Values of NPA Charge and Fukui Indices on Individual Atoms of Functional PMDA Corrosion Inhibitors. The Atomic-Level Numbers Are Represented as per the Given Schematic Structure of Inhibitors

Inh1				inh2				inh3			
Atom	NPA	f^+	f^-	Atom	NPA	f^+	f^-	Atom	NPA	f^+	f^-
1C	-0.10	0.05	0.070	1C	-0.10	0.03	0.07	1C	-0.10	-0.01	0.07
2C	-0.15	0.00	-0.005	2C	-0.15	0.01	-0.00	2C	-0.15	0.01	-0.01
3C	-0.10	0.05	0.070	3C	-0.10	-0.00	0.07	3C	-0.10	0.01	0.06
4C	-0.10	0.05	0.070	4C	-0.10	-0.00	0.07	4C	-0.10	0.01	0.06
5C	-0.15	0.00	-0.006	5C	-0.15	0.01	-0.00	5C	-0.15	0.01	-0.01
6C	-0.10	0.05	0.070	6C	-0.10	0.03	0.07	6C	-0.10	-0.01	0.07
7C	0.70	-0.01	0.046	7C	0.70	-0.00	0.04	7C	0.70	-0.00	0.04
8N	-0.49	0.15	0.006	8N	-0.49	0.06	0.01	8N	-0.49	0.01	0.01
9C	0.70	-0.02	0.046	9C	0.70	-0.00	0.04	9C	0.70	-0.00	0.04
10O	-0.54	0.08	0.093	10O	-0.54	0.04	0.09	10O	-0.54	0.02	0.08
11O	-0.54	0.07	0.093	11O	-0.54	0.04	0.09	11O	-0.54	0.02	0.08
12C	-0.47	-0.01	-0.009	12C	-0.27	0.03	-0.00	12C	-0.27	-0.00	-0.01
13C	0.70	-0.02	0.046	13C	-0.26	-0.00	-0.00	13C	-0.26	-0.00	-0.00
14N	-0.49	0.15	0.006	14N	-0.89	0.28	0.00	14N	-0.89	0.02	0.00
15C	0.70	-0.01	0.046	15C	0.70	-0.00	0.04	15C	0.70	0.01	0.04
16O	-0.54	0.08	0.093	16N	-0.49	0.02	0.00	16N	-0.49	-0.01	0.01
17O	-0.544	0.075	0.093	17C	0.700	-0.006	0.045	17C	0.70	0.01	0.04
18C	-0.47	-0.01	-0.01	18O	-0.54	0.03	0.09	18O	-0.54	0.00	0.09
				19O	-0.54	0.03	0.09	19O	-0.54	0.00	0.09
				20C	-0.47	-0.01	-0.01	29C	-0.31	0.15	0.01
								30C	-0.31	0.15	0.01
								31C	0.19	0.04	0.02
								33C	0.19	0.04	0.01
								35C	-0.33	-0.03	0.02
								36N	-0.83	0.11	0.01
								40N	-0.83	0.11	0.01

ΔN value for inh3 (0.246) shows the transfer of an electron from the surface. Thus, greater ΔN for inh3 represents an excess electron transfer to the inhibitor, resulting in strong adsorption.

The natural population analysis (NPA) charge and Fukui indices on individual atoms of F-PMDI inhibitors are listed in Table 2. N, O, and few C atoms carry a more negative charge (center), while the rest of the C atoms take a more positive charge (center). At the negative charge center, electrons could be offered to the surface to form a coordinate bond, while the positive charge center can accept the free electrons of the metallic surface. In inh3, greater negative/positive charge centers provide strong adsorption by forming coordinate bonds. The Fukui indices f^- and f^+ control the electrophilic and nucleophilic attacks. Greater f^- and f^+ of an atom indicate an electrophilic and nucleophilic attack, respectively. The nitrogen atom is found to be the most preferable center for nucleophilic attack. The high nitrogen element composition in inh3 (~ 19.17%) compared to that in inh1 (~11.47%) and inh2 (~15.38%) provides a larger nucleophilic attack site, resulting in the strong adsorption of inh3 on the surface compared to that of inh1 and inh2.

Till now, we have discussed the corrosion resistance properties of F-PMDI inhibitors in gas phase. Further, we have investigated the corrosion inhibition parameters of F-PMDI in aqueous (water) media, which are also listed in Table 1. E_{HOMO} and E_{LUMO} of F-PMDI are slightly reduced in aqueous media compared to that in gas phase. For example, E_{HOMO} and E_{LUMO} of the inh3 inhibitor show reduction up to 0.08 and 0.04 eV, respectively. ΔE_{gap} values of inh1, inh2, and inh3 are found to be 4.39, 3.54, and 2.25 eV, respectively, which are slightly smaller (up to ~0.06) than that in gas phase. In fact, the reduction of ΔE_{gap} for inh3 in aqueous media is negligible (0.03 eV) compared to that in the gas phase. Similarly, absolute electronegativity, hardness and softness, and fraction of electron transferred show very small changes for F-PMDI (especially for inh3) in aqueous media. It is found that the dipole moment reduces for inh1 (from 0.63 to 0.07 D),

https://doi.org/10.1021/acsomega.2c01299
ACS Omega XXXX, XXX, XXX−XXX

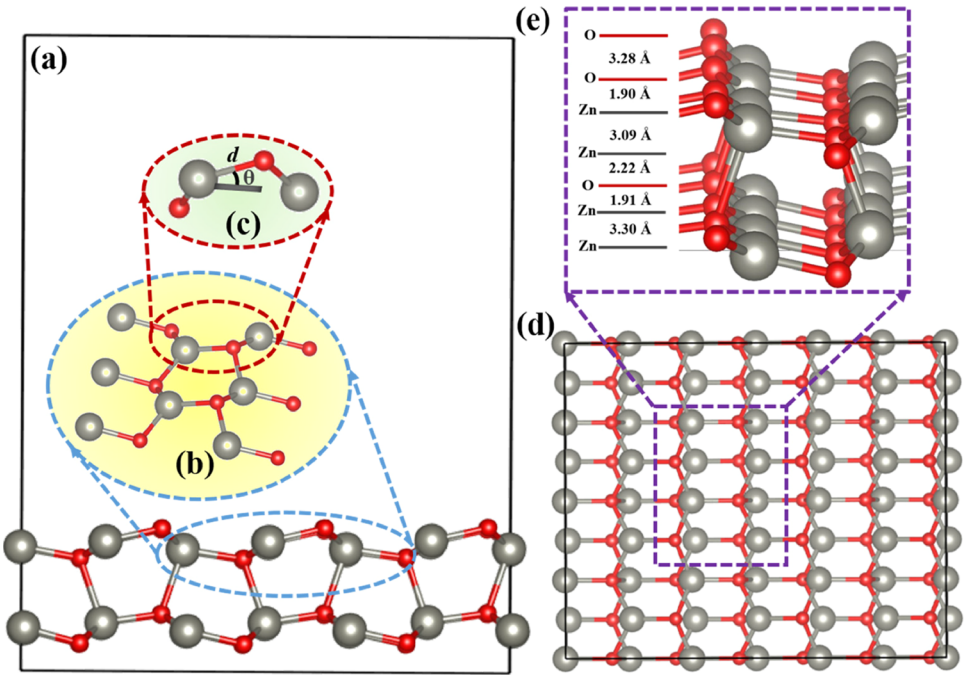

Figure 3. (a) Side view (d) top view of the relaxed structure of ZnO($10\bar{1}0$) surface. (b,c) Small region of the ZnO($10\bar{1}0$)surface. (e) Interatomic and interlayer distances of the ZnO layer. The Zn and O atoms are represented by silver and red spheres, respectively.

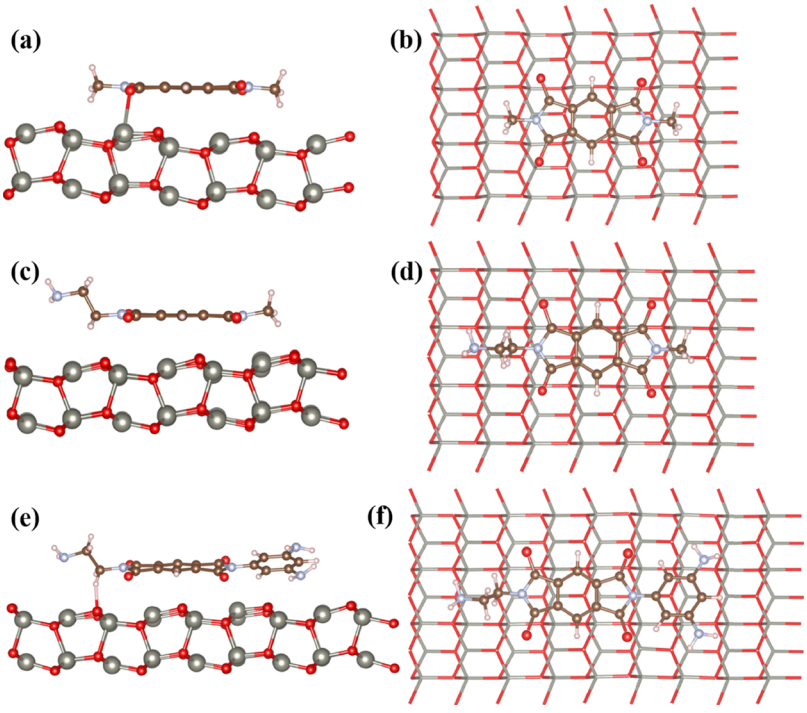

Figure 4. Side views (left panel) of the optimized structures of adsorbed (a) inh1, (c) inh2, and (e) inh3 above the ZnO($10\bar{1}0$) surface. The figures in the right panel (b,d,f) represent the corresponding top views. In the top view, the surface atoms are represented by the tube model, while the ball−stick model shows inhibitor atoms for a better viewership. The Zn, O, C, N, and H atoms are represented by silver, red, brown, gray silver, and white spheres, respectively.

while it enhances for inh2 (1.49 to 1.87 D) and inh3 (2.26 to 2.97 D) in aqueous media compared to that in gas media. The analysis of corrosion resistance parameters in both phases shows that aqueous media do not affect the inhibition performance order of F-PMDI. In both, that is, gaseous and aqueous phases, the inhibition performance order of inhibitors is inh3 > inh2 > inh1.

3.2. F-PMDI Inhibitor Adhesion on ZnO ($10\bar{1}0$) Surface. The lattice constants 3.24 and 5.19 Å of ZnO ($10\bar{1}0$) are found to be in excellent agreement with 3.25 and 5.20 Å, respectively, of the experimental results.[45−47] The interlayer spacing and interatomic distances of relaxed ZnO ($10\bar{1}0$) are depicted in Figure 3. Equal amounts of Zn and O per unit area in ZnO ($10\bar{1}0$) are required for breaking only one

https://doi.org/10.1021/acsomega.2c01299
ACS Omega XXXX, XXX, XXX−XXX

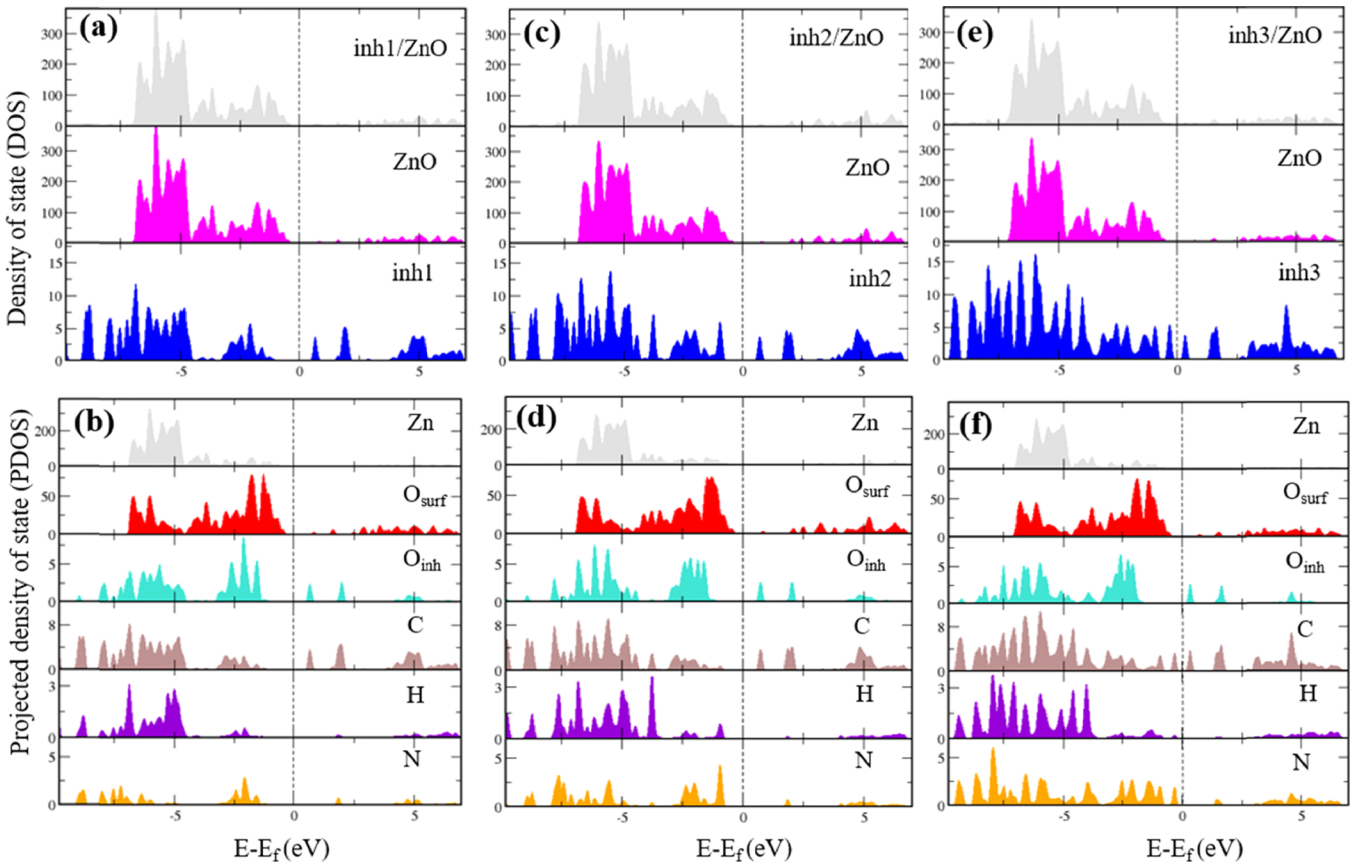

Figure 5. (a,b) DOS and PDOS of the inh1/ZnO($10\bar{1}0$) system. (c) DOS and (d) PDOS of the inh2/ZnO($10\bar{1}0$) system. (e) DOS and (f) PDOS of the inh3/ZnO($10\bar{1}0$) system. The Fermi levels are set at 0 eV and represented by vertical dashed gray lines.

bond per atom for the surface growth, hence auto-compensated. One dangling bond per atom in step-edge O and Zn atoms forms a dimer row (consisting of a Zn−O chain) running along the *z*-direction and creates a rectangular terrace on top of the surface. Each surface Zn/O atom is bonded with two atoms (O and Zn) in the surface layer and one atom (O and Zn) in the second layer. The distances between planar atoms, for example, ∼3.28 Å (O−O), ∼3.30 Å (Zn−Zn), and 1.90 Å (Zn−O), and the layer atoms of ZnO($10\bar{1}0$), for example, ∼3.20 Å (O−O), ∼3.10 Å (Zn−Zn), and ∼ 2.22 Å (Zn−O), are in good agreement with the previous report.[47]

The inhibitors oriented horizontally (PMDI parallel to the surface) on ZnO ($10\bar{1}0$) to cover the maximum surface and larger contact regions. Further, horizontal orientation is also found as a preferable position through HOMO distribution, MEP surface, and Fukui functions (electrophilic/nucleophilic centers arising on N and O atoms). Relaxed F-PMDI with ZnO ($10\bar{1}0$) is depicted in Figure 4. A significant distortion (split into two sublayers) on the outermost ZnO($10\bar{1}0$) layer arises during the adsorption with inhibitors. For example, in the ZnO−inh3 system, few surface Zn and O atome were displaced toward the adhesion region. Zn bonded with N and O_{inh} (of the inhibitor), while O_{surf} bonded with N and H (of the inhibitor), enhancing the adsorption strength during the interaction between the inhibitor and ZnO($10\bar{1}0$) surface. Due to the repulsion between O_{surf} and O_{inh}, few Zn and O atoms are displaced away from the adhesion region, resulting in the reduction in adsorption strength. The adsorption energy (E_{ads}) is found to be −119.66, −122.56, and −182 kJ/mol for inh1, inh2, and inh3, respectively. With greater E_{ads}, inh3 is found to be a superior corrosion inhibitor, also consistent with quantum chemical results. An additional aromatic ring (m-phenylenediamine) in inh3 provides a larger surface to interact. The E_{ads} value on the ZnO surface will be lower than that on the bulk Zn surface due to the charge shielding of Zn by O_{surf} atom, resulting in a comparatively weaker interaction. The minimum distance between surface Zn (O_{surf}) and N is 3.01 (2.92) Å, 3.13 (3.02) Å, and 2.90 (3.22) Å, while that between Zn and O_{inh} is 2.38, 2.81, and 2.42 Å for inh1, inh2, and inh3, respectively. Here, the bond length does not directly relate with E_{ads} due to the complex interplay between the different atomic orbitals of the inhibitor and ZnO($10\bar{1}0$) surface. The adsorption nature (physisorption or chemisorption) of the inhibitor on the surface could not be directly predicted with E_{HOMO}, E_{gap}, ΔN, or E_{ads}.[48] To determine the adsorption/bonding nature of the F-PMDI inhibitor on the ZnO($10\bar{1}0$) surface, we have investigated the orbital contribution through the density of states (DOS) and projected density of states (PDOS).

Figure 5 shows the DOS and PDOS of individual F-PMDI inhibitors, ZnO ($10\bar{1}0$) surface, and inhibitor/ZnO($10\bar{1}0$) system. In the bare ZnO ($10\bar{1}0$), the valence band (VB) is primarily composed of O-2p and Zn-3d states, with a little contribution from Zn-3p states. This agrees with the ultraviolet photoemission spectroscopy results where the Zn-3d core level localized below the Fermi energy, whereas O-p and Zn-3d orbitals dominate VB.[49] The conduction band (CB) comprises O-2p and Zn-3p states, with Zn-4s states for the lowest CB in bare ZnO($10\bar{1}0$). The deeper VB region of inhibitors is composed of O-2p and C-2p states, with a small contribution

https://doi.org/10.1021/acsomega.2c01299
ACS Omega XXXX, XXX, XXX−XXX

from the H-1s and N-2s states of the inhibitors. In the VB range −5 to 0 eV, there is a lack of states available in inh1, while comparatively more states are available in inh2 and inh3. In fact, few states are available near the Fermi level in inh3. PDOS analysis suggests that VB (in the range −5 to 0 eV) is composed of N-2p state, with a small contribution from H-1s states. The orbital states of inhibitors that lie at the ZnO (Zn-d and O-p states) states can be considered to describe the inhibitor−surface bonding upon adsorption. In inh2, N-2p states are available near −2.5 eV along with a small H-1s state, which shows an overlap in the states of Zn and O_{surf}. In inh3, more states (of N) are available, including the presence of N-2p state near the Fermi level showing the overlap with the Zn-3d state. Therefore, strong interaction occurs between N (of inh3) and Zn (of ZnO $(10\bar{1}0)$) with the formation of the dative bond. Furthermore, comparatively more states are available for H of inh3 than inh1/inh2. This H-1s state overlaps with the available states of O_{surf}, providing a strong interaction betweeen H (of inh3) and O_{surf} (of ZnO$(10\bar{1}0)$) through hydrogen-bond formation. These characters are reflected when the inhibitors are adsorbed on ZnO$(10\bar{1}0)$ (DOS of inhibitor/ZnO system in Figure 5), and the peaks (states' contribution of inhibitor) are slightly broadened due to hybridization between the inhibitor and Zn/O (of surface) states. In the VB range −7.5 to −5 eV, the inhibitor's O-2p state lies on Zn states, resulting in an interaction between O_{inh} and Zn, which is also reflected in the DOS of all inhibitor/ZnO$(10\bar{1}0)$ systems. However, greater available states for N and H of inh3 lie at the states of Zn and O_{surf}, respectively, leading to N−Zn dative-bond formation and H−O_{surf} hydrogen-bond formation. These bonds are only formed in inh3 and are additional to the O_{inh}−Zn bond, which appears in all inhibitors. To further probe into the bonding nature, we have investigated the redistribution of charge density in the vicinity of adsorbed inhibitors and ZnO$(10\bar{1}0)$ surface.

The charge density difference ($\Delta\rho(\mathbf{r}) = \rho_{inh/surf}(\mathbf{r}) - \rho_{surf}(\mathbf{r}) - \rho_{inh}(\mathbf{r})$) of F-PMDI inhibitor in the most stable adsorption configuration with ZnO$(10\bar{1}0)$ is shown in Figure 6. The strength of the bonding of the inhibitor to ZnO$(10\bar{1}0)$ could be understood by the formation of dative and hydrogen bonds. In the inh1/ZnO system, the Zn−O_{inh} bond (d = 2.38 Å) can be observed by the charge density redistribution (accumulation (yellow color) on O_{suf} and depletion (cyan color) on Zn) between Zn and O_{inh}, that is, charge flow toward the Zn−O_{inh} center (see Figure 6a). This dative bond formed due to electron donation from the lone pair of O_{inh} to Zn has a comparatively lower binding strength than the ionic bond, Zn−O_{surf} (present on the ZnO$(10\bar{1}0)$ surface). This is verified by bond length analysis, where the length of the Zn−O_{surf} bond (∼1.90 Å) is smaller than that of the Zn−O_{inh} bond (d = 2.38 Å). In the inh2/ZnO system, the lack of charge density accumulation/depletion between Zn and O_{inh} leads to no formation of the Zn−O_{inh} bond (as d = 3.26 Å) (see Figure 6b). Further, charge density depleted below H, although sufficient charge density is not accumulated over O_{surf}, showing the lack of H bonding. However, the bond distance between H(1)−O_{surf}, H(2)−O_{surf}, and H(1)−O_{surf} is 2.19 Å, 2.82, and 2.40 Å, respectively, showing partial H-bonding. In inh3, excess charge density accumulation/depletion between Zn (surface) and N/O_{inh} (inhibitor) shows the dative Zn−N and Zn−O_{inh} bond formation (see Figure 6c). Further, the H bonding is confirmed by the charge density accumulation on O_{surf} and charge density depletion on H(s) of inh3. This is confirmed by the bond length analysis, where H(1)−O_{surf}, H(2)−O_{surf}, and H(3)−O_{surf} are 2.32, 2.41, and 2.07 Å, respectively. Thus, the presence of both dative bond (Zn−N and Zn−O_{inh}) and H-bond (H−O_{surf}) between inh3 and ZnO$(10\bar{1}0)$ leads to stronger adsorption in comparison to inh1 and inh2.

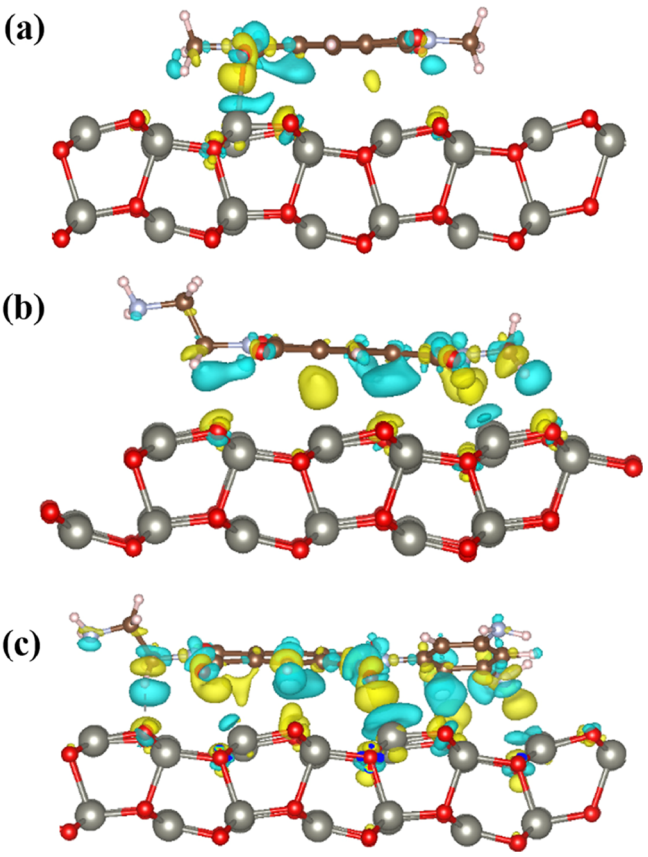

Figure 6. Charge density difference of (a) inh1, (b) inh2, and (c) inh3 on the ZnO$(10\bar{1}0)$ surface. Electron accumulation and depletion regions are represented by yellow and cyan colors, respectively (isosurface = 0.001 e/Å^3). Hence, a charge redistribution is observed when the inhibitor interacts with the ZnO$(10\bar{1}0)$ surface, and the charge moves from the $-\Delta\rho$ (cyan) region to the $+\Delta\rho$ (yellow) region. The redistribution of charges is more prominent in the case of inh3, which leads to a stronger interaction between inh3 and the ZnO$(10\bar{1}0)$ surface.

4. CONCLUSIONS

Using density functional theory, we have investigated the corrosion resistance performance of F-PMDI on galvanized steel. The corrosion resistance parameters such as E_{HOMO}, E_{LUMO}, ΔE_{gap}, electronegativity, dipole moment, global hardness and softness, and the fraction of electron transfer (ΔN) have been studied through quantum chemical calculations. The obtained results indicate the superior corrosion inhibition performance of inh3 (R = $-C_6H_3(NH_2)_2$, R′ = $-CH_2CH_2NH_2$) compared to inh1 (R = $-CH_3$, R′ = $-CH_3$) and inh2 (R = $-CH_3$, R′ = $-CH_2CH_2NH_2$) in the order of inh3 > inh2 > inh1. Further, we have studied the adsorption of F-PMDI on ZnO$(10\bar{1}0)$ substrate and found that inh3 (182.38 kJ/mol) possesses a high adsorption energy compared to that of inh2 (122.56 kJ/mol) and inh1 (119.66 kJ/mol). The origin of the superior performance of inh3 has been probed through charge transfer, DOS, and PDOS. The larger available states for N- and H of inh3 lie at Zn and O_{surf},

https://doi.org/10.1021/acsomega.2c01299
ACS Omega XXXX, XXX, XXX−XXX

respectively, leading to N−Zn and H−O_{surf} bond formation. These bonds are only formed in inh3 and are additional to the O_{inh}−Zn bond which appears in all inhibitors. The bonding nature is further confirmed by charge density difference analysis, where the excess charge density accumulation/depletion between Zn/O_{surf} (of the substrate) and N/O_{inh}/H (of inh3) shows the formation of dative and hydrogen bonds. Inh3 strongly adsorbs on the ZnO($10\bar{1}0$) surface through chemisorption. In short, this study suggests that by using the inh3 (based on F-PMDI) inhibitor, the corrosion resistance performance of galvanized steel can be enhanced significantly. We hope that this work would motivate researchers to synthesize inh3 inhibitors to be applied in industry. It should be pointed out that few F-PMDI such as pyridinium-F-PMDI and phosphonium-F-PMDI have been synthesized and widely used in several applications.[50,51]

AUTHOR INFORMATION

Corresponding Author

Saroj Kumar Nayak − *School of Basic Sciences, Indian Institute of Technology Bhubaneswar, Khordha 752050 Odisha, India;* orcid.org/0000-0001-6570-8964; Email: nayaks@iitbbs.ac.in

Authors

Anoop Kumar Kushwaha − *School of Basic Sciences, Indian Institute of Technology Bhubaneswar, Khordha 752050 Odisha, India;* orcid.org/0000-0002-6258-1635

Mihir Ranjan Sahoo − *School of Basic Sciences, Indian Institute of Technology Bhubaneswar, Khordha 752050 Odisha, India; Harish-Chandra Research Institute, HBNI, Prayagraj 211019 Uttar Pradesh, India;* orcid.org/0000-0002-5528-7657

Mausumi Ray − *Research and Development, Tata Steel Limited, Jamshedpur 831007, India*

Debashish Das − *School of Basic Sciences, Indian Institute of Technology Bhubaneswar, Khordha 752050 Odisha, India*

Suryakanta Nayak − *Research and Development, Tata Steel Limited, Jamshedpur 831007, India*

Apurba Maity − *Research and Development, Tata Steel Limited, Jamshedpur 831007, India*

Kuntal Sarkar − *Research and Development, Tata Steel Limited, Jamshedpur 831007, India*

Amar Nath Bhagat − *Research and Development, Tata Steel Limited, Jamshedpur 831007, India*

Atanu Ranjan Pal − *Research and Development, Tata Steel Limited, Jamshedpur 831007, India*

Tapan Kumar Rout − *Research and Development, Tata Steel Limited, Jamshedpur 831007, India*

Complete contact information is available at: https://pubs.acs.org/10.1021/acsomega.2c01299

Author Contributions

‖A.K.K., M.R.S. and M.R. have equal contribution.

Author Contributions

A.K.K. (ak20@iitbbs.ac.in): calculation, investigation and analysis, writing, and conceptualization; M.R.S. (mrs10@iitbbs.ac.in): calculation, investigation and analysis, writing, and conceptualization; M.R. (mausumi.ray@tatasteel.com): conceptualization and manuscript review; D.D. (das.debashish37@gmail.com): calculation and investigation and analysis; S.N. (suryakanta.nayak@tatasteel.com): conceptualization; A.M. (apurba.maity@tatasteel.com) conceptualization; K.S. (kuntal.sarkar@tatasteel.com): conceptualization; A.N.B. (anbhagat@tatasteel.com): conceptualization; A.R.P. (atanu1@tatasteel.com): conceptualization;, T.K.R. (tapankumarrout@tatasteel.com): conceptualization and manuscript review; S.K.N. (nayaks@iitbbs.ac.in): supervision, conceptualization, analysis, manuscript review and editing, and funding acquisition.

Notes

The authors declare no competing financial interest.

ACKNOWLEDGMENTS

We would like to acknowledge the funding agencies, Tata Steel Ltd., Consultancy project (CP240; entitled: *Design and formulation of coating using molecular modeling and simulation*), MHRD Centre of Excellence for Novel Energy Material (CENEMA: RP-074). The simulations and/or computations were supported by SAMKHYA: High-Performance Computing Facility provided by the Institute of Physics, Bhubaneswar.

REFERENCES

(1) Cole, I. S. Recent Progress and Required Developments in Atmospheric Corrosion of Galvanised Steel and Zinc. *Materials* **2017**, *10*, 1288.

(2) Illiberi, A.; Roozeboom, F.; Poodt, P. Spatial Atomic Layer Deposition of Zinc Oxide Thin Films. *ACS Appl. Mater. Interfaces* **2012**, *4*, 268−272.

(3) Basiaga, M.; Walke, W.; Kajzer, W.; Sambok-Kiełbowicz, A.; Szewczenko, J.; Simka, W.; Szindler, M.; Ziębowicz, B.; Lubenets, V. Atomic Layer Deposited ZnO Films on Stainless Steel for Biomedical Applications. *Arch. Civil Mech. Eng.* **2021**, *21*, 1−15.

(4) Wang, D.; Unsal, T.; Kumseranee, S.; Punpruk, S.; Mohamed, M. E.; Saleh, M. A.; Gu, T. Sulfate Reducing Bacterium Desulfovibrio Vulgaris Caused Severe Microbiologically Influenced Corrosion of Zinc and Galvanized Steel. *Int. Biodeterior. Biodegrad.* **2021**, *157*, No. 105160.

(5) Yadav, A. P.; Katayama, H.; Noda, K.; Masuda, H.; Nishikata, A.; Tsuru, T. Effect of Fe−Zn Alloy Layer on the Corrosion Resistance of Galvanized Steel in Chloride Containing Environments. *Corros. Sci.* **2007**, *49*, 3716−3731.

(6) Li, X.; Zhang, D.; Liu, Z.; Li, Z.; Du, C.; Dong, C. Materials Science: Share Corrosion Data. *Nat. News* **2015**, *527*, 441.

(7) Javaherdashti, R. How Corrosion Affects Industry and Life. *Anti-Corros. Methods Mater.* **2000**, *47*, 30.

(8) Hansson, C. M. The Impact of Corrosion on Society. *Metall. Mater. Trans. A* **2011**, *42*, 2952−2962.

(9) He, J.; Lian, J.; Aretz, A.; Vajragupta, N.; Hangen, U.; Goodwin, F.; Münstermann, S. Fracture Properties of Zinc Coating Layers in a Galvannealed Steel and an Electrolytically Galvanized Steel. *Mater. Sci. Eng., A* **2018**, *732*, 320−325.

(10) Trabanelli, G. *Corrosion Mechanisms*, Mansfeld, F., Ed.; Marcel Dekker: New York, 1987.

(11) Singh, A. K. Inhibition of Mild Steel Corrosion in Hydrochloric Acid Solution by 3-(4-((Z)-Indolin-3-Ylideneamino) Phenylimino) Indolin-2-One. *Ind. Eng. Chem. Res.* **2012**, *51*, 3215−3223.

(12) Ashassi-Sorkhabi, H.; Majidi, M. R.; Seyyedi, K. Investigation of Inhibition Effect of Some Amino Acids against Steel Corrosion in HCl Solution. *Appl. Surf. Sci.* **2004**, *225*, 176−185.

(13) Ahamad, I.; Prasad, R.; Quraishi, M. A. Inhibition of Mild Steel Corrosion in Acid Solution by Pheniramine Drug: Experimental and Theoretical Study. *Corros. Sci.* **2010**, *52*, 3033−3041.

(14) Khaled, K. F. Corrosion Control of Copper in Nitric Acid Solutions Using Some Amino acids−A Combined Experimental and Theoretical Study. *Corros. Sci.* **2010**, *52*, 3225−3234.

(15) Bentiss, F.; Traisnel, M.; Gengembre, L.; Lagrenée, M. A New Triazole Derivative as Inhibitor of the Acid Corrosion of Mild Steel: Electrochemical Studies, Weight Loss Determination, SEM and XPS. *Appl. Surf. Sci.* **1999**, *152*, 237−249.

https://doi.org/10.1021/acsomega.2c01299
ACS Omega XXXX, XXX, XXX−XXX

(16) Guo, L.; Obot, I. B.; Zheng, X.; Shen, X.; Qiang, Y.; Kaya, S.; Kaya, C. Theoretical Insight into an Empirical Rule about Organic Corrosion Inhibitors Containing Nitrogen, Oxygen, and Sulfur Atoms. *Appl. Surf. Sci.* **2017**, *406*, 301−306.
(17) Kaya, S.; Guo, L.; Kaya, C.; Tüzün, B.; Obot, I. B.; Touir, R.; Islam, N. Quantum Chemical and Molecular Dynamic Simulation Studies for the Prediction of Inhibition Efficiencies of Some Piperidine Derivatives on the Corrosion of Iron. *J. Taiwan Inst. Chem. Eng.* **2016**, *65*, 522−529.
(18) Kumar, C. B. P.; Mohana, K. N.; Muralidhara, H. B. Electrochemical and Thermodynamic Studies to Evaluate the Inhibition Effect of Synthesized Piperidine Derivatives on the Corrosion of Mild Steel in Acidic Medium. *Ionics* **2015**, *21*, 263−281.
(19) Ousslim, A.; Bekkouch, K.; Chetouani, A.; Abbaoui, E.; Hammouti, B.; Aouniti, A.; Elidrissi, A.; Bentiss, F. Adsorption and Corrosion Inhibitive Properties of Piperidine Derivatives on Mild Steel in Phosphoric Acid Medium. *Res. Chem. Intermed.* **2014**, *40*, 1201−1221.
(20) Lavanya, K.; Saranya, J.; Chitra, S. Recent Reviews on Quinoline Derivatives as Corrosion Inhibitors. *Corros. Rev.* **2018**, *36*, 365−371.
(21) Mert, B. D.; Mert, M. E.; Kardaş, G.; Yazıcı, B. Experimental and Theoretical Investigation of 3-Amino-1, 2, 4-Triazole-5-Thiol as a Corrosion Inhibitor for Carbon Steel in HCl Medium. *Corros. Sci.* **2011**, *53*, 4265−4272.
(22) Errahmany, N.; Rbaa, M.; Abousalem, A. S.; Tazouti, A.; Galai, M.; Touhami, M. E.; Lakhrissi, B.; Touir, R. Experimental, DFT Calculations and MC Simulations Concept of Novel Quinazolinone Derivatives as Corrosion Inhibitor for Mild Steel in 1.0 M HCl Medium. *J. Mol. Liq.* **2020**, *312*, No. 113413.
(23) Agustín-Sáenz, C.; Martín-Ugarte, E.; Jorcin, J. B.; Imbuluzqueta, G.; Santa Coloma, P.; Izagirre-Etxeberria, U. Effect of Organic Precursor in Hybrid Sol−gel Coatings for Corrosion Protection and the Application on Hot Dip Galvanised Steel. *J. Sol-Gel Sci. Technol.* **2019**, *89*, 264−283.
(24) Pokhmurs'Kyi, V. I.; Lyon, S. B. Inhibition of Corrosion by a Mixture of Nonchromate Pigments in Organic Coatings on Galvanized Steel. *Mater. Sci.* **2004**, *40*, 383−390.
(25) Zin, I. M.; Lyon, S. B.; Pokhmurskii, V. I. Corrosion Control of Galvanized Steel Using a Phosphate/calcium Ion Inhibitor Mixture. *Corros. Sci.* **2003**, *45*, 777−788.
(26) Montemor, M. F.; Simões, A. M.; Ferreira, M. G. S.; Williams, B.; Edwards, H. The Corrosion Performance of Organosilane Based Pre-Treatments for Coatings on Galvanised Steel. *Prog. Org. Coat.* **2000**, *38*, 17−26.
(27) Wint, N.; Griffiths, C. M.; Richards, C. J.; Williams, G.; McMurray, H. N. The Role of Benzotriazole Modified Zinc Phosphate in Preventing Corrosion-Driven Organic Coating Disbondment on Galvanised Steel. *Corros. Sci.* **2020**, *174*, No. 108839.
(28) Al-Azzawi, A. M.; Hammud, K. K. Newly Antibacterial/anti-Rusting Oxadiazole Poromellitic Di-Imids of Carbon Steel/hydrochloric Acid Interface: Temkin Isother Model. *Int. J. Res. Pharm. Chem.* **2016**, *6*, 391−402.
(29) Guo, X.; Watson, M. D. Pyromellitic Diimide-Based Donor−acceptor Poly (Phenylene Ethynylene) S. *Macromolecules* **2011**, *44*, 6711−6716.
(30) Haque, J.; Verma, C.; Srivastava, V.; Quraishi, M. A.; Ebenso, E. E. Experimental and Quantum Chemical Studies of Functionalized Tetrahydropyridines as Corrosion Inhibitors for Mild Steel in 1 M Hydrochloric Acid. *Results Phys.* **2018**, *9*, 1481−1493.
(31) Galai, M.; Rbaa, M.; Ouakki, M.; Abousalem, A. S.; Ech-Chihbi, E.; Dahmani, K.; Dkhireche, N.; Lakhrissi, B.; EbnTouhami, M. Chemically Functionalized of 8-Hydroxyquinoline Derivatives as Efficient Corrosion Inhibition for Steel in 1.0 M HCl Solution: Experimental and Theoretical Studies. *Surf. Interfaces* **2020**, *21*, No. 100695.
(32) Islam, M. M.; Diawara, B.; Marcus, P.; Costa, D. Synergy between Iono-Covalent Bonds and van Der Waals Interactions in SAMs Formation: A First-Principles Study of Adsorption of Carboxylic Acids on the Zn−ZnO (0 0 0 1) Surface. *Catal. Today* **2011**, *177*, 39−49.
(33) Maddahi, P. S.; Shahtahmassebi, N.; Roknabadi, M. R.; Moosavi, F. Site Specific Interaction of Aromatic Amino Acids with ZnO Nanotubes: A Density Functional Approach. *Comput. Theor. Chem.* **2016**, *1086*, 36−44.
(34) Wei, M.; Li, C.-F.; Deng, X.-R.; Deng, H. Surface Work Function of Transparent Conductive ZnO Films. *Energy Procedia* **2012**, *16*, 76−80.
(35) Becke, A. D. Completely Numerical Calculations on Diatomic Molecules in the Local-Density Approximation. *Phys. Rev. A* **1986**, *33*, 2786.
(36) Lee, C.; Yang, W.; Parr, R. G. Development of the Colle-Salvetti Correlation-Energy Formula into a Functional of the Electron Density. *Phys. Rev. B* **1988**, *37*, 785.
(37) Frisch, M. J.; Trucks, G. W.; Schlegel, H. B.; Scuseria, G. E.; Robb, M. A.; Cheeseman, J. R.; Scalmani, G.; Barone, V.; Mennucci, B.; Petersson, G. A. *Gaussian 09*; Gaussian, Inc.: Wallingford, CT, 2009; Vol. *32*, pp 5648−5652.
(38) Kresse, G.; Furthmüller, J. Efficient Iterative Schemes for Ab Initio Total-Energy Calculations Using a Plane-Wave Basis Set. *Phys. Rev. B* **1996**, *54*, 11169.
(39) Kresse, G.; Furthmüller, J. Efficiency of Ab-Initio Total Energy Calculations for Metals and Semiconductors Using a Plane-Wave Basis Set. *Comput. Mater. Sci.* **1996**, *6*, 15−50.
(40) Kresse, G.; Joubert, D. From Ultrasoft Pseudopotentials to the Projector Augmented-Wave Method. *Phys. Rev. B* **1999**, *59*, 1758.
(41) Adamo, C.; Barone, V. Toward Reliable Density Functional Methods without Adjustable Parameters: The PBE0 Model. *J. Chem. Phys.* **1999**, *110*, 6158−6170.
(42) Perdew, J. P.; Burke, K.; Ernzerhof, M. Generalized Gradient Approximation Made Simple. *Phys. Rev. Lett.* **1996**, *77*, 3865.
(43) Monkhorst, H. J.; Pack, J. D. Special Points for Brillouin-Zone Integrations. *Phys. Rev. B* **1976**, *13*, 5188.
(44) Lu, T.; Chen, F. Multiwfn: A Multifunctional Wavefunction Analyzer. *J. Comput. Chem.* **2012**, *33*, 580−592.
(45) Flores, E. M.; Moreira, M. L.; Piotrowski, M. J. Structural and Electronic Properties of Bulk ZnX (X= O, S, Se, Te), ZnF2, and ZnO/ZnF2: A DFT Investigation within PBE, PBE+ U, and Hybrid HSE Functionals. *J. Phys. Chem. A* **2020**, *124*, 3778−3785.
(46) Sawada, H.; Wang, R.; Sleight, A. W. An Electron Density Residual Study of Zinc Oxide. *J. Solid State Chem.* **1996**, *122*, 148−150.
(47) Cooke, D. J.; Marmier, A.; Parker, S. C. Surface Structure of (1010) and (1120) Surfaces of ZnO with Density Functional Theory and Atomistic Simulation. *J. Phys. Chem. B* **2006**, *110*, 7985−7991.
(48) Kokalj, A. Corrosion Inhibitors: Physisorbed or Chemisorbed? *Corros. Sci.* **2021**, 109939.
(49) Powell, R. A.; Spicer, W. E.; McMenamin, J. C. Photoemission Studies of Wurtzite Zinc Oxide. *Phys. Rev. B* **1972**, *6*, 3056.
(50) Greenlee, A. J.; Ofosu, C. K.; Xiao, Q.; Modan, M. M.; Janzen, D. E.; Cao, D. D. Pyridinium-Functionalized Pyromellitic Diimides with Stabilized Radical Anion States. *ACS Omega* **2018**, *3*, 240−245.
(51) Kim, M. J.; Luo, S. M.; Greenlee, A. J.; Young, V. G., Jr.; Cao, D. D. A Highly Stabilized Phosphonium Ylide That Forms Supramolecular Dimers in Solution and the Solid State. *Chem. − Eur. J.* **2019**, *25*, 15257−15261.

https://doi.org/10.1021/acsomega.2c01299
ACS Omega XXXX, XXX, XXX−XXX